

Highly Repeatable and Cyclically Stable Mechanoluminescence of the Flexible Composite Elastomer

Shaofan Fang, Lusi Zhao, Xiao He, Bo Zhou, Yongwen He, Zhibin Lu, and Zhaofeng Wang*

Mechanoluminescence (ML) elastomer shows tremendous potential for the next generation of flexible displaying, imaging, and sensing devices. However, inadequate repeatability and cyclic stability are the current bottlenecks. In this work, a solid-solution strategy is reported to regulate the interfacial interactions of ML elastomer, in which the $(\text{Ca,Ba})_5(\text{PO}_4)_3\text{Cl}:\text{Eu}$ solid solutions and polydimethylsiloxane (PDMS) are employed, respectively. The results suggest that the solid-solution strategy can effectively modulate the energy position of the valence band and the charge density distributions of the lowest unoccupied band, as well as the interfacial triboelectrification. Consequently, the ML performance of the composite elastomer in terms of intensity, spectral characteristic, and repeatability has been significantly improved. Particularly, the optimum $\text{CaBa}_4(\text{PO}_4)_3\text{Cl}:\text{Eu}/\text{PDMS}$ elastomer exhibits stable and repeatable ML for over 20 000 cycles under various rapid and continuous stretching conditions. This work not only provides a highly repeatable and cyclically stable ML elastomer but also clarifies the intrinsic physical principles, showing high guiding significance for future ML design and applications.

matrix can directly endow the elastomer with attractive mechanics-optics conversion characteristics. On one hand, the ML elastomer exhibits remarkable functionality, which can utilize the natural energy, such as the energy of wind, tide, and human motion, to trigger the luminescent displaying and imaging with no consumption of the secondary energy.^[3–7] On the other hand, the emitted light signal conveys a wealth of mechanical information, which can be in situ and wirelessly captured for intelligent monitoring and sensing.^[8–17] Therefore, the ML elastomer simultaneously possesses the advantages of simplicity, functionality, and intellectuality, which shows tremendous potential toward the next generation of wearable devices, artificial intelligent skin, biomechanics detection, information encryption, and human-computer interaction.^[18–27]

To date, a variety of material systems have been developed to exhibit ML with

1. Introduction

Mechanoluminescence (ML) elastomer is a type of flexible composite material that can emit light when stimulated by mechanics, such as rubbing, compressing, stretching, impacting, etc.^[1,2] In ML elastomer, no circuit design is introduced. The simple structure composed of inorganic phosphors and polymer

abundant colors, and the underlying physical principles have also been extended from the energy pre-stored type to the self-charged and self-recovered one.^[28–36] These achievements bring significant confidence for researchers to prompt the practical applications of ML materials. At present, one of the biggest performance limitations of ML materials lies in the repeatability and cyclic stability, particularly the ones under high mechanical frequency with continuous stimuli. To the best of our knowledge, for the ML elastomer material under stretching stimulation, ZnS:Cu/polydimethylsiloxane (ZnS:Cu/PDMS) is the reported one that has remarkable repeatability and cyclic stability over 10 000 cycles under the rapid and continuous stretching conditions.^[37–39] This is because ZnS:Cu is a special alternating current electroluminescence (EL) material, and the observed ML is actually the EL under the triboelectrification between ZnS:Cu and PDMS.^[40–43] For this unique reason, although the outstanding ML performance of ZnS:Cu/PDMS has been known for several decades, researchers still cannot achieve a second ML elastomer with similar performance. Providing one can establish a general physical principle and develop a novel composite elastomer to overcome the current bottlenecks in terms of ML repeatability and cyclic stability, it would have great significance in the development history of ML.

Although the coupling of the interfacial triboelectricity and EL is unique for the ZnS:Cu/PDMS elastomer, the previous

S. Fang, L. Zhao, X. He, B. Zhou, Z. Wang
 Shandong Laboratory of Advanced Materials and Green Manufacturing
 at Yantai
 Yantai, Shandong 264006, China
 E-mail: zhfwang@licp.cas.cn

Y. He, Z. Lu, Z. Wang
 State Key Laboratory of Solid Lubrication
 Lanzhou Institute of Chemical Physics
 Chinese Academy of Sciences
 Lanzhou, Gansu 730000, China

Y. He, Z. Lu, Z. Wang
 Center of Materials Science and Optoelectronics Engineering
 University of Chinese Academy of Sciences
 Beijing 100049, China

 The ORCID identification number(s) for the author(s) of this article can be found under <https://doi.org/10.1002/adma.202505071>

DOI: 10.1002/adma.202505071

research also suggested that there should be other physical pathways to bridge the interfacial triboelectricity and ML.^[44–46] In 2022, by combining the ML properties with the electron transfer direction during friction, our group proposed a possible interfacial triboelectrification-induced electron bombardment (ITEB) model to specifically describe the physical processes from the interfacial triboelectricity to the generation of ML.^[47] Following this model, a series of self-recoverable ML composite elastomers, e.g., the PDMS-based ones with $\text{Sr}_3\text{Al}_2\text{O}_5\text{Cl}_2:\text{Dy}^{3+}$,^[48] $\text{Ca}_9\text{Bi}(\text{PO}_4)_7:\text{Ce}^{3+}$,^[49] $\text{Ca}_6\text{BaP}_4\text{O}_{17}:\text{Ce}^{3+}$,^[50] $\text{Sr}_5(\text{PO}_4)_3\text{Cl}:\text{Eu}^{2+}$,^[51] and $\text{Ca}_9\text{Al}(\text{PO}_4)_7:\text{Ce}^{3+}$,^[52] have been developed. Theoretically, the ML achieved by the ITEB model should be mechanically repeatable and cyclically stable. However, due to the degradation of the interfacial interactions in terms of the possible hydrogen bond, Van der Waals' force, and the triboelectrification under continuous and cyclic stimuli, the ML always rapidly decreased and disappeared within several cycles.^[47–52] When prolonging the interval time of the cycles (from tens of minutes to several hours), the degraded interfacial interactions can be partially restored, and thus the ML elastomer in this case can exhibit a certain repeatability with slow self-recoverability.

After finding out the critical factor in terms of the interface self-repairability, it is supposed that the ITEB model should be effective in developing the highly repeatable and cyclically stable ML elastomer as long as the phosphors can establish desirable interfacial interactions with the polymer matrix. Inspired by this research thought, in this work, we developed a series of ML composites by combining the $(\text{Ca},\text{Ba})_5(\text{PO}_4)_3\text{Cl}:\text{Eu}$ (CBPOCE) solid solution materials with the flexible PDMS. Here, the double anion structure of $\text{A}_5(\text{PO}_4)_3\text{Cl}:\text{Eu}$ ($\text{A} = \text{Ca}$ or Ba) was employed, because of its abundant anionic characteristics in terms of polarizability and electronegativity, as well as the flexibility for local lattice distortion and crystalline field adjustment.^[53–56] The solid solution strategy is supposed to further enhance the interface match ability for the phosphor particles with the PDMS chains. The results suggest that the solid-solution strategy of the CBPOCE can effectively regulate the ML performance of the composites in terms of intensity, spectral characteristics, and repeatability. Particularly, the optimum $\text{Ca}_4\text{Ba}(\text{PO}_4)_3\text{Cl}:\text{Eu}/\text{PDMS}$ elastomer exhibits stable and repeatable ML for over 20 000 cycles under various rapid and continuous stretching conditions. As a result, this work achieves the long-term searching ML elastomer with high repeatability and cyclic stability after $\text{ZnS}:\text{Cu}/\text{PDMS}$, and the corresponding physical mechanisms in terms of the ML generation and the solid-solution regulation are proposed.

2. Results and Discussion

2.1. Solid-Solution Regulation

The CBPOCE, i.e., $\text{Ca}_5(\text{PO}_4)_3\text{Cl}:\text{Eu}$, $\text{Ba}_5(\text{PO}_4)_3\text{Cl}:\text{Eu}$, and their solid solutions, were synthesized by a solid-state reaction. The X-ray diffraction (XRD) patterns in **Figure 1a** match well with the referenced standard card of $\text{Ca}_5(\text{PO}_4)_3\text{Cl}$ (JCPDS no.73-1728) and $\text{Ba}_5(\text{PO}_4)_3\text{Cl}$ (JCPDS no.70-2318) without impurity peaks. With the increase of the content of Ba^{2+} , the patterns of the CBPOCE gradually shift toward a low-angle side because of the larger ionic radius of Ba^{2+} . The $\text{Ca}_5(\text{PO}_4)_3\text{Cl}$ and $\text{Ba}_5(\text{PO}_4)_3\text{Cl}$ both belong to the hexagonal phase with a space group of $P6_3/m$ (No.176). In

the crystal structure of $\text{Ca}_5(\text{PO}_4)_3\text{Cl}$ (**Figure 1b**), there are two independent crystallographic Ca sites, named Ca1 and Ca2, respectively. The Ca1 occupies the 4f site with C_3 point symmetry coordinated by nine O_2^- to form the $[\text{CaO}_9]$ tetrakaidekahedron, and the Ca2 occupies the 6h site with C_s point symmetry coordinated by six O_2^- and two Cl^- to form $[\text{CaO}_6\text{Cl}_2]$ hendecahedron.^[53] Significantly, the Cl^- anions define the boundaries of the unit cell, indicating that Cl^- anions are more likely to be exposed on the surface. When the luminescent centers of Eu^{2+} ions were doped in the structure of CBPOCE, they were supposed to occupy the $\text{Ca}^{2+}/\text{Ba}^{2+}$ sites according to the similarity of ionic radius and valence. The scanning electron microscope (SEM) image and energy dispersive spectrometer (EDS) mappings in **Figure S1** (Supporting Information) suggest that the obtained CBPOCE particles have a size of ca. 10 μm with the Ca, Ba, P, O, Cl, and Eu elements distributed. The above results confirm that the pure CBPOCE micron-sized particles have been successfully synthesized.

The photoluminescence (PL) performance of the prepared CBPOCE with different Ca/Ba ratios was investigated, as shown in **Figure S2** (Supporting Information). The $\text{Ca}_5(\text{PO}_4)_3\text{Cl}:\text{Eu}$ has an emission peak at 465 nm belonging to the transition of $4f^65d^1 \rightarrow 4f^7$ of Eu^{2+} .^[57,58] It can be observed that an additional PL peak at 498 nm appears when some Ba^{2+} ions substitute Ca^{2+} ions. When all Ca^{2+} ions are replaced by Ba^{2+} ions, the product $\text{Ba}_5(\text{PO}_4)_3\text{Cl}:\text{Eu}$ exhibits an emission peak at 443 nm. The above evolution in terms of the PL spectra should be attributed to the effect of the adjustable crystal field owing to the difference in ionic radius of Ca^{2+} and Ba^{2+} .^[57] **Figure 1c** shows the ML spectra of the as-prepared CBPOCE by incorporating the particles into the PDMS elastomer. The ML spectra in terms of the radiative transitions of Eu^{2+} are similar to the PL ones, although their excitation/activation sources are different. With the increase of the Ba^{2+} proportion in the solid-solutions of CBPOCE, the ML peak of Eu^{2+} gradually shifts from 460 to 498 nm due to the distortion of Ca^{2+} and Ba^{2+} sites. However, there are some weak ML peaks at ca. 585, 613, 647, and 692 nm, attributing to the transitions of $^5\text{D}_0 \rightarrow ^7\text{F}_j$ ($j = 0, 1, 2, 3, 4$) of Eu^{3+} , respectively.^[59] This is due to the chemical pressure produced by the ion substitution with different ionic radii, which prevents the reduction of a part of Eu^{3+} ions.^[59] In addition to the spectral shape evolution, the ML intensity of the CBPOCE exhibits a rapid enhancement with the increase of the Ba content, as shown in **Figure 1d**. The ML intensity of the $\text{CaBa}_4(\text{PO}_4)_3\text{Cl}:\text{Eu}$ is 15.7 times that of the $\text{Ca}_5(\text{PO}_4)_3\text{Cl}:\text{Eu}$, and 1.5 times that of the $\text{Ba}_5(\text{PO}_4)_3\text{Cl}:\text{Eu}$, demonstrating that the coexistence of Ca and Ba in the solid solutions can significantly improve the ML performance. To explore the contribution of the solid-solution strategy on ML performance, the density functional theory (DFT) calculations were performed. **Figure S3** (Supporting Information) shows that the valence band (VB) of the samples with mixed cations moves toward the Fermi level (the Fermi level is shifted to 0.00 eV), whereas the conduction band (CB) of all samples remains stationary relative to the Fermi level. The elevated energy position of the peak near the Fermi level suggests a reduced energy barrier for electron excitation, and the enhanced peak intensity suggests a higher population of electrons in VB for excitation,^[60] which are compared quantitatively in **Figure 1e**. When the ratio of Ca: Ba reaches 1: 4, the $\text{CaBa}_4(\text{PO}_4)_3\text{Cl}:\text{Eu}$ shows both a high energy position and high

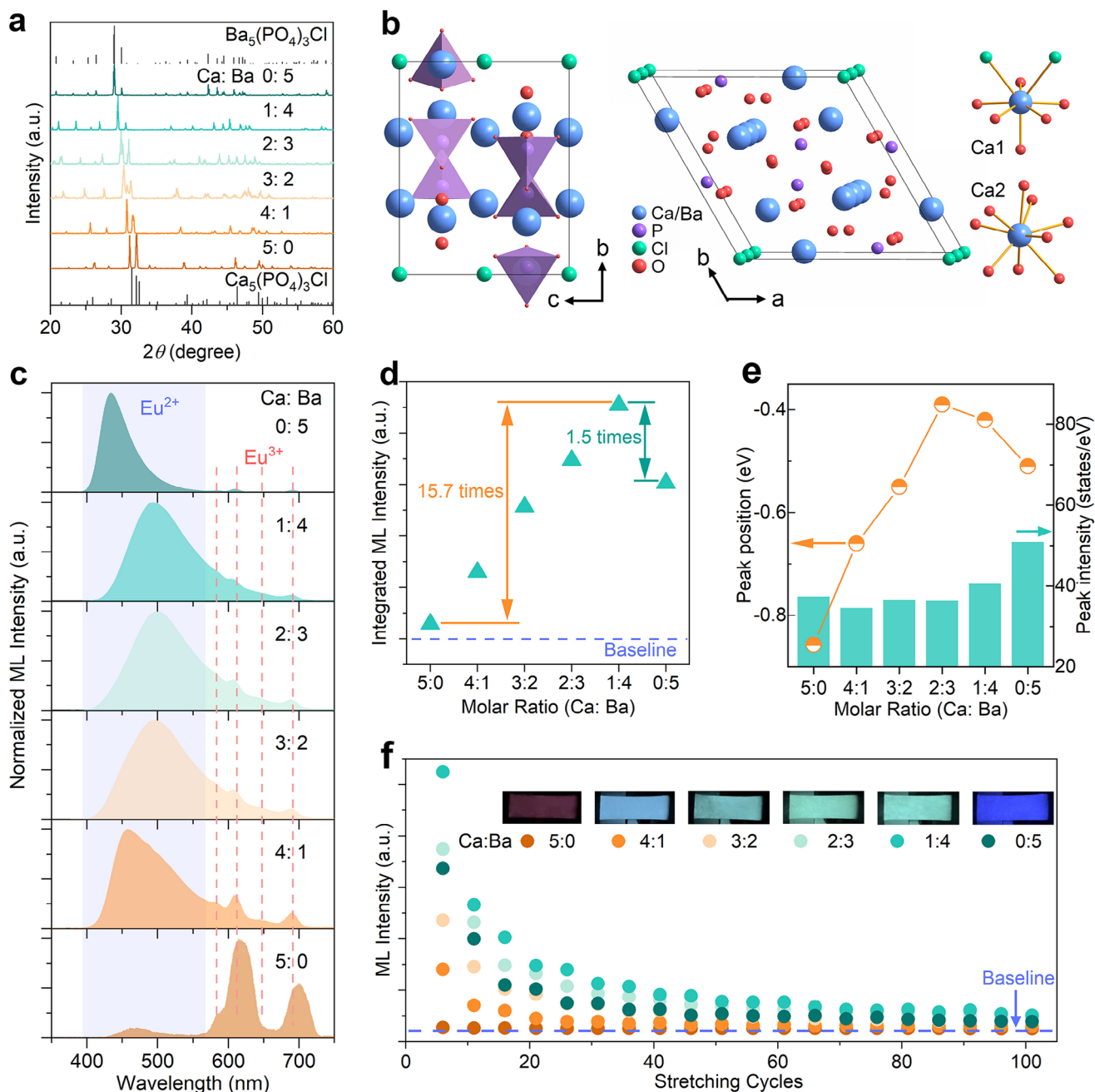


Figure 1. Structure, PL, and ML regulations. a) XRD patterns of the prepared CBPOCE powders with various Ca/Ba ratios. b) Schematic diagram of the crystal structure and the coordination polyhedra. c) Normalized ML spectra and d) integrated ML intensity of the CBPOCE samples with various Ca/Ba ratios. e) Variations of the energy position and peak intensity near the Fermi level from the density of state (DOS) of the CBPOCE samples. f) Repeatability test of the composite elastomers for 100 stretching cycles (strain: 50%; frequency: 5 Hz; no pre-stretching was applied for this test).

peak intensity, which could facilitate electrons to be excited to CB under the same excitation/activation conditions. Therefore, the largely enhanced ML of the $CaBa_4(PO_4)_3Cl:Eu$ is closely related to its intrinsic electronic structure.

In addition to the ML peak and intensity variations, the Ca:Ba ratios of the CBPOCE solid solutions also exhibit a significant influence on ML repeatability, as shown in Figure 1f. Like most of the ML elastomers the $Ca_5(PO_4)_3Cl:Eu/PDMS$ can ex-

hibit ML just for the initial cycles under continuous stretching. Attractively, with the introduction of Ba^{2+} in $Ca_5(PO_4)_3Cl:Eu$ to form solid-solutions, the ML repeatability is greatly enhanced, i.e., the CBPOCE samples except the $Ca_5(PO_4)_3Cl:Eu$ all show over 100 repetitions in PDMS under the stretching conditions of 5 Hz and 50% strain. Among them, the ML of the $CaBa_4(PO_4)_3Cl:Eu/PDMS$ exhibits the highest ML intensity during the entire cyclic process. As a result, the solid-solution

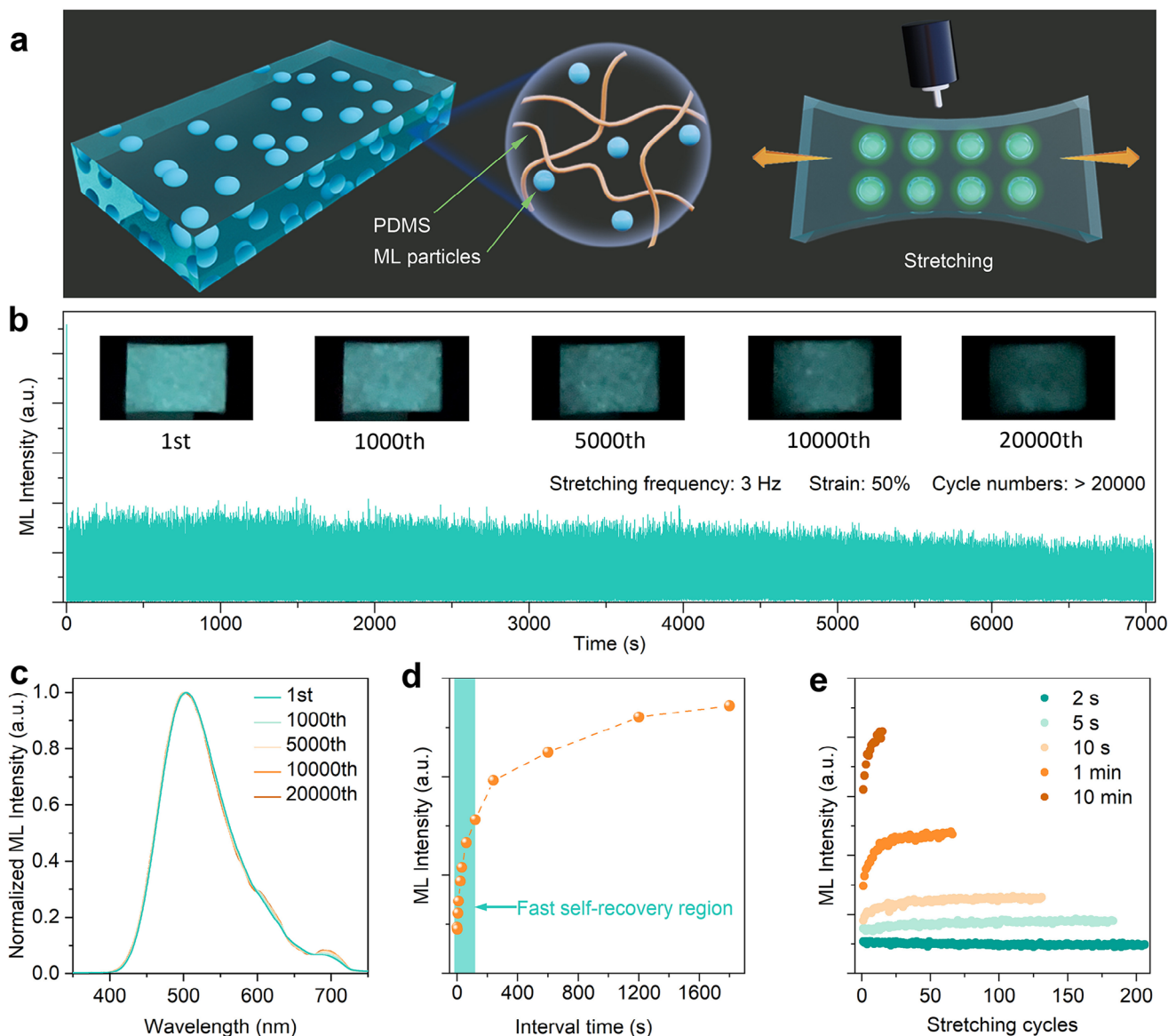


Figure 2. Self-recoverability and repeatability of the composite elastomer. a) Schematic illustration of the fabricated CBPOCE/PDMS composite elastomer. b) Stability and repeatability tests of the composite elastomer over 20 000 stretching cycles (strain: 50%; frequency: 3 Hz). The insets are the ML photographs of the composite elastomer at different stretching cycles. c) The ML spectra of the $\text{CaBa}_4(\text{PO}_4)_3\text{Cl:Eu/PDMS}$ at different stretching cycles. d) Self-recovery test of the composite elastomer after placing for different times under dark and ambient temperature. e) Repeatability test of the ML of the $\text{CaBa}_4(\text{PO}_4)_3\text{Cl:Eu/PDMS}$ with various time intervals between the successive cycles. To avoid the interference of the initial degradation by interfacial break and traps, a pre-stretching of 1000 cycles was applied in (b), (d), and (e).

strategy by introducing Ba^{2+} in $\text{Ca}_5(\text{PO}_4)_3\text{Cl:Eu}$ is confirmed to be effective in regulating the ML performance in terms of the intensity, spectral characteristic, and repeatability, and the optimum sample is determined as the one with the Ca: Ba ratio of 1:4.

2.2. Rapidly Self-Recoverable and Highly Repeatable ML

It should be noted that the powders of the CBPOCE themselves cannot emit ML if they were stimulated by any mechan-

ics like grinding, impacting, or compressing. When the powders were composited into the flexible PDMS, intense ML can be achieved, as illustrated in **Figures 2a** and **S4** (Supporting Information). This indicates that the interfacial interactions between the CBPOCE particles and the PDMS chains should play critical roles in the ML generation. Moreover, different from the previous reports, no pre-irradiation was required to produce the ML of the CBPOCE/PDMS composite elastomer. It suggests that the ML of the CBPOCE/PDMS should mainly belong to the mechanical self-activation type which brings great practicability and convenience in real scenarios. The cyclic stability and repeatability are

particularly important to determine the practical applications of the ML materials toward the new generation of flexible displaying, imaging, and sensing devices. At present, there is one elastomer, ZnS:Cu/PDMS, can exhibit repeatable ML under continuous stretching over 10 000 times. ZnS:Cu is a very special material that is a low-threshold alternating current electroluminescence material. The ML of ZnS:Cu in PDMS should come from a variety of electric field stimuli from triboelectricity.^[40–43] Thus, it is difficult to find another ML elastomer to have the highly repeatable ML with the same physical mechanisms with ZnS:Cu. Here, we achieve the highly repeatable and cyclically stable ML in the $\text{CaBa}_4(\text{PO}_4)_3\text{Cl:Eu}$ /PDMS composite elastomer. Figures 2b and Figure S5 (Supporting Information) depict the ML intensity evolution of the $\text{CaBa}_4(\text{PO}_4)_3\text{Cl:Eu}$ /PDMS over 20 000 mechanical cycles under the continuous stretching mode with different strains and frequencies (a pre-stretching of 1000 cycles was applied to avoid the interference by the interfacial broken and intrinsic traps at the initial stage). The corresponding visualization effect under the continuous stretching is presented in Movies S1 and S2 (Supporting Information). The ML intensity is attenuated at the first stage, which may be due to the break of the hydrogen bonds and van der Waals forces at the interfaces between the powders and the PDMS chains. Then, the ML intensity is stabilized, and the ML after 20 000 stretching cycles is still visible to the naked eye. Figure 2c shows the normalized ML spectra of the $\text{CaBa}_4(\text{PO}_4)_3\text{Cl:Eu}$ /PDMS elastomer at various stretching cycles (1st, 1000th, 5000th, 10 000th, and 20 000th). They exhibit the same spectral characteristics, further suggesting the ML cyclic stability of the $\text{CaBa}_4(\text{PO}_4)_3\text{Cl:Eu}$ /PDMS.

As discussed in Figure 2b, the elastomer would experience the break of the hydrogen bonds and van der Waals forces, resulting in the ML intensity attenuation at the first stage.^[61] Since the above interfacial interactions could be partially self-repaired, the ML of the $\text{CaBa}_4(\text{PO}_4)_3\text{Cl:Eu}$ /PDMS composite elastomer exhibits adjustable self-recovery activities. Figure 2d shows the ML self-recovery degrees with various placing times in dark under ambient temperature. Before the test, the elastomer was continuously pre-stretched for 1000 cycles to reach the stable ML. The placing time shows remarkable influence on the stabilized ML intensity under continuous stimuli, which exhibits a logarithmic relationship. In Figure 2d, there is a fast self-recovery region within 120 s at room temperature. By further prolonging the placing time, the restored ML intensity can be slowly enhanced. These results confirm that the ML of the $\text{CaBa}_4(\text{PO}_4)_3\text{Cl:Eu}$ /PDMS elastomer exhibits the placing time-dependent self-recovery activities. It suggests that the intensity of the stabilized ML during continuous stretching cycles can be readily adjusted by controlling the time intervals between the successive cycles. As shown in Figure 2e, the ML intensity under continuous stretching is largely adjusted with the time interval changed from 2 s to 5 s, 10 s, 1 min, and 10 min, providing great flexibility for various applications.

2.3. ML Physics and Regulation Mechanisms

From a macro scale, ML realizes the physical conversion from mechanics to light. Since the emission light has been intrinsically demonstrated from the radiative electron transfer of lumi-

nescent centers, there should be a close relationship between the macroscopic mechanics and the microscopic electrons which determines the ML performance. To reveal this relationship in the CBPOCE/PDMS composite elastomer, the electronic behaviors related to the trap structure, piezoelectricity, and triboelectricity were investigated. Here, the optimum sample $\text{CaBa}_4(\text{PO}_4)_3\text{Cl:Eu}$ is taken as a representative. Figure 3a shows the thermoluminescence (TL) spectra of $\text{CaBa}_4(\text{PO}_4)_3\text{Cl:Eu}$ after pre-heat-treatment at various temperatures. The pristine $\text{CaBa}_4(\text{PO}_4)_3\text{Cl:Eu}$ exhibits a multimodal TL spectra, suggesting the presence of both shallow and deep traps within the structure. With the increase of the pre-heat-treatment temperature, the carriers are gradually cleared from shallow traps to deep traps. The trapped carriers can be fully cleaned at the temperature of 673 K for 10 min. However, the $\text{CaBa}_4(\text{PO}_4)_3\text{Cl:Eu}$ in this case can still exhibit distinct ML in the flexible PDMS matrix. The $\text{CaBa}_4(\text{PO}_4)_3\text{Cl:Eu}$ /PDMS sample with the trapped carriers fully released also exhibits good ML repeatability as shown in Figure 3c. Obviously, the remained ML after thermal treatment should be independent of the traps. When the phosphor with cleaned traps was re-charged by an ultraviolet (UV) light, the trap density exhibited a time-dependent increase (Figure S6, Supporting Information). After such UV re-charging for ≈ 10 min, the trap structures of $\text{CaBa}_4(\text{PO}_4)_3\text{Cl:Eu}$ could be almost restored. Correspondingly, the UV re-charging activity leads to a remarkable ML enhancement compared to the one with cleaned traps, as shown in Figure 3b. This demonstrates that the enhanced ML after UV re-charging should be attributed to the trap-controlled mechanisms. The above results and discussion suggest that the trapped carriers in the structure should be the partial origination of ML, which could affect the intensity during initial cycles. This is also one of the reasons for the initial ML degradation during the repeatability test. However, the retained ML after pre-treating at 673 K for 10 min with no trapped carriers suggests that there should be another ML origination which is the real cause for the repeatable and stable ML of the $\text{CaBa}_4(\text{PO}_4)_3\text{Cl:Eu}$ /PDMS composite elastomer.

The ML of the $\text{CaBa}_4(\text{PO}_4)_3\text{Cl:Eu}$ exhibits a high dependency on the composite matrices, as shown in Figure 3d. For the $\text{CaBa}_4(\text{PO}_4)_3\text{Cl:Eu}$ powders or their epoxy resin (ER) based composites, no emission can be found under rubbing, scratching, compressing, or impacting. Since the pressure stress dominates the above mechanical processes, the absent ML in these cases suggests that the piezoelectricity should not be involved in the ML generation.^[48,50,51] On the contrary, when the $\text{CaBa}_4(\text{PO}_4)_3\text{Cl:Eu}$ powders are embedded into some flexible matrices, such as PDMS and silica gel (SG), ML could be produced (the ones within PDMS and SG have strong and weak ML, respectively). However, the $\text{CaBa}_4(\text{PO}_4)_3\text{Cl:Eu}$ incorporated into the flexible polyurethane (PU) still has no ML. Therefore, the ML of the $\text{CaBa}_4(\text{PO}_4)_3\text{Cl:Eu}$ could be produced in the flexible composites, which depends on the types of the matrices.

Relative to the pressure stress in the hard composites, the interfacial rubbing actions should dominate in the flexible composites during stretching, because of its large deformation and large relative displacement between powders and matrices. Accordingly, the triboelectric properties of the $\text{CaBa}_4(\text{PO}_4)_3\text{Cl:Eu}$ rubbed with different polymer matrices were investigated. As shown in Figure 3e and Figure S7 (Supporting Information), after rubbing with $\text{CaBa}_4(\text{PO}_4)_3\text{Cl:Eu}$ for 1 min under 120 rpm,

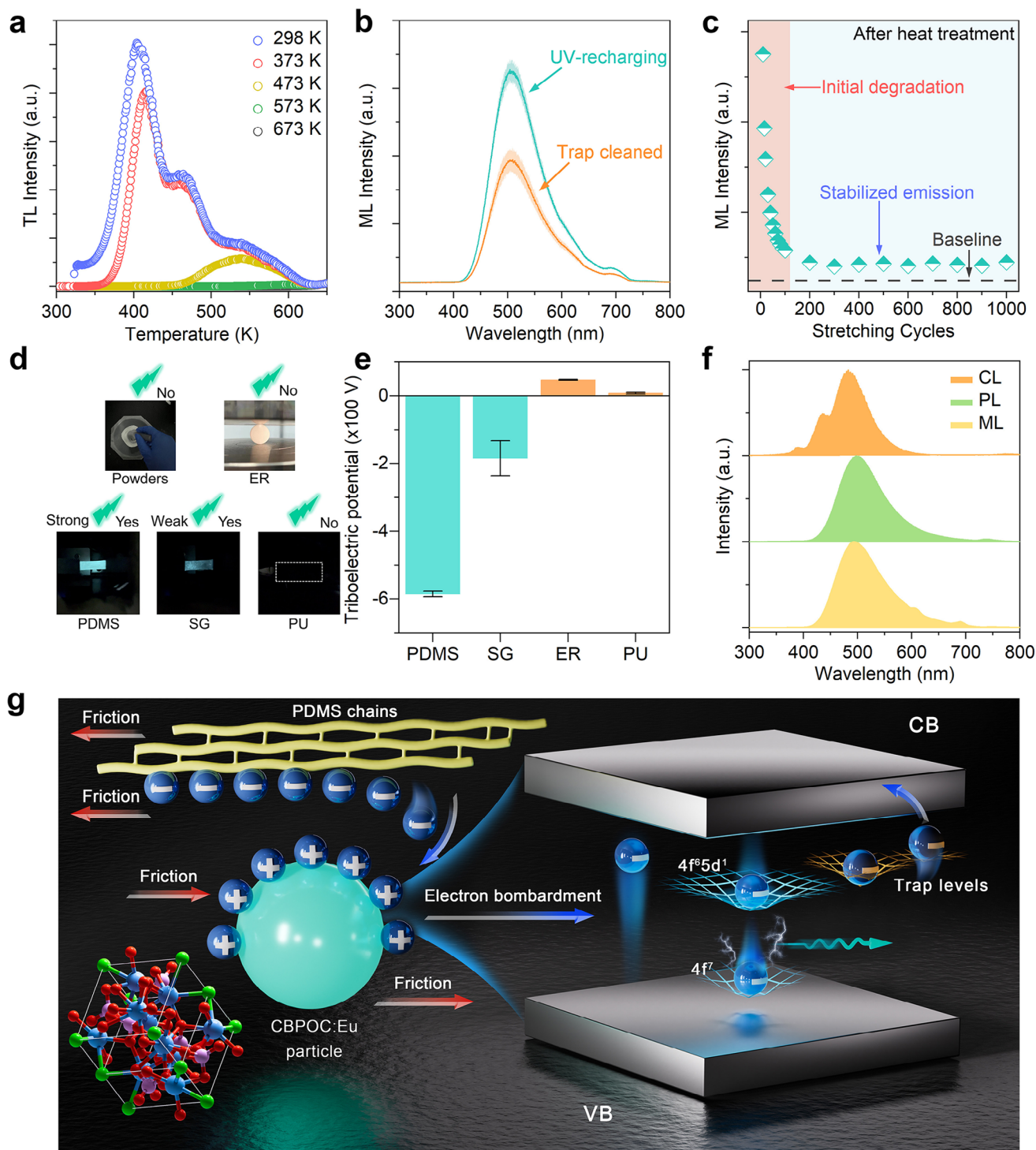


Figure 3. Physical mechanisms for ML. a) TL spectra of the $\text{CaBa}_4(\text{PO}_4)_3\text{Cl:Eu}$ after heat treatment at different temperatures. b) ML spectra of the $\text{CaBa}_4(\text{PO}_4)_3\text{Cl:Eu/PDMS}$ with or without UV re-charging for 10 min after the CBPOCE powders heated at 673 K for 10 min. c) Repeatability of the $\text{CaBa}_4(\text{PO}_4)_3\text{Cl:Eu/PDMS}$ after the powders heated at 673 K for 10 min without UV charging (no pre-stretching was applied). d) Photographs and ML photos of the $\text{CaBa}_4(\text{PO}_4)_3\text{Cl:Eu}$ samples in various forms. e) Triboelectric potential of the PDMS, SG, ER, and PU after rubbing with the $\text{CaBa}_4(\text{PO}_4)_3\text{Cl:Eu}$ under 120 rpm for 1 min. f) Comparison of the CL, PL, and ML spectra of the $\text{CaBa}_4(\text{PO}_4)_3\text{Cl:Eu/PDMS}$. g) Schematic diagram of the proposed ML mechanism.

the PDMS and SG show negative potential, while the ER and PU exhibit positive potential. The electron transfer pathways during the triboelectrification between the $\text{CaBa}_4(\text{PO}_4)_3\text{Cl}:\text{Eu}$ and the matrices are consistent with the ML phenomena, i.e., the sample can exhibit ML when it is incorporated into the matrix with negative triboelectric potential. Therefore, the ML of $\text{CaBa}_4(\text{PO}_4)_3\text{Cl}:\text{Eu}$ should be related to the interfacial triboelectricity with the matrix, but it is different from the triboelectricity-induced EL of $\text{ZnS}:\text{Cu}$ that the $\text{CaBa}_4(\text{PO}_4)_3\text{Cl}:\text{Eu}$ makes request on the electron transfer direction during triboelectrification. The investigation of ML behaviors during a single stretching cycle in Figure S8 (Supporting Information) further confirms the above viewpoint that the ML of $\text{CaBa}_4(\text{PO}_4)_3\text{Cl}:\text{Eu}/\text{PDMS}$ should come from the interfacial triboelectricity with obvious difference to $\text{ZnS}:\text{Cu}/\text{PDMS}$. Figure 3f shows the cathodoluminescence (CL) spectrum of the $\text{CaBa}_4(\text{PO}_4)_3\text{Cl}:\text{Eu}$ under the electron beam excitation (accelerating voltage: 10 kV; filament current: 10 mA). The basic spectral characteristics are consistent with the ML ones, with slight shoulder peaks at 389 and 435 nm due to their excitation energy difference.^[62] The obtained CL of $\text{CaBa}_4(\text{PO}_4)_3\text{Cl}:\text{Eu}$ suggests that there is high energy electron bombardment pathway to excite the phosphor. By comprehensively combining the trap dependency, the matrix effects, the triboelectricity analyses, as well as the CL characteristics, the achieved ML of the $\text{CaBa}_4(\text{PO}_4)_3\text{Cl}:\text{Eu}$ in PDMS should partially come from the trapped carriers, and another part should be the ITEB, in which the latter is the real reason for the highly self-activated, stable and repeatable ML. The trap-related mechanism has been well explained in previous research,^[28] and the ML physical processes in terms of ITEB are proposed as follows. As illustrated in Figure 3g, first, under mechanical stimuli, the interfacial friction makes the electrons transferred from $\text{CaBa}_4(\text{PO}_4)_3\text{Cl}:\text{Eu}$ particles to PDMS chains, causing the generation of the interfacial triboelectric field. Then, the electrons on the surface of PDMS are bombarded to the $\text{CaBa}_4(\text{PO}_4)_3\text{Cl}:\text{Eu}$ particles under the interfacial triboelectric field, during which the electrons in $\text{CaBa}_4(\text{PO}_4)_3\text{Cl}:\text{Eu}$ are excited from VB to CB. The excited electrons further transfer to the $4f^65d^1$ energy levels of the luminescence center Eu^{2+} ions. Finally, the electrons in $4f^65d^1$ levels radiatively transfer to the $4f^7$ levels of Eu^{2+} by emitting photons, producing the as-observed ML. Under continuous stretching, the entire ML processes of $\text{CaBa}_4(\text{PO}_4)_3\text{Cl}:\text{Eu}/\text{PDMS}$ can be repeated with no need for additional input energy.

The above results and discussions confirm that the interfacial triboelectricity between the phosphors and the polymer matrix as well as the electron excitation possibility play critical roles on the repeatable ML. To further understand the solid-solution regulation mechanisms in this work, the triboelectric properties and the intrinsic electronic structures of the CBPOCE solid solutions are specifically investigated. Figure 4a shows the surface triboelectric potentials of the PDMS after rubbing with the CBPOCE series with different Ca/Ba ratios. The triboelectric potentials on PDMS exhibit a similar variation trend to that of the ML intensity in Figure 1d that it increases first and then decreases with the maximum value at the Ca/Ba ratio of 1:4. Therefore, one of the solid-solution regulation reasons should be the adjustment of the triboelectric properties between the CBPOCE and PDMS. In addition, the partial density of states (PDOS) of the CBPOCE solid solutions is also calculated, as presented in Figure

S9 (Supporting Information). The VB is mainly contributed by O and Cl atoms, and their energy position and peak intensity near the Fermi level dependent on the Ca/Ba ratios are quantitatively summarized in Figure 4b,c. Based on the PDOS proportion, the regulation of the energy position and peak intensity of O atoms is supposed to be the primary contribution to the enhanced ML by solid solution. Compared to O atoms, Cl atoms exhibit a higher energy position. Moreover, the position variation of Cl atoms in Figure 4c exhibits a closer correlation with the ML intensity change. Therefore, the VB structure in terms of Cl in CBPOCE should be also crucial for the ML generation from the electron excitation aspect, which could be facilely adjusted by altering the Ca/Ba ratios in CBPOCE. Figure 4d further shows the band-decomposed charge density distributions of the lowest unoccupied band of the CBPOCE solid solutions with various Ca/Ba ratios, which are primarily contributed by Ca and Ba atoms. For $\text{Ca}_5(\text{PO}_4)_3\text{Cl}:\text{Eu}$, the charge density distribution of the lowest unoccupied band is relatively dispersed. However, with the introduction and increase of the Ba content, the charge density is gradually localized and confined around Cl atoms, which may provide more efficient pathways for charge transfer from VB to CB leading to enhanced ML. Therefore, the above theoretical investigations suggest that in addition to the interfacial triboelectric properties of the CBPOCE/PDMS composite elastomer, the adjustment of the energy position of VB near the Fermi level and the charge density distribution of the lowest unoccupied band is also responsible for the enhanced ML via solid-solution regulation. These regulations endow the $\text{CaBa}_4(\text{PO}_4)_3\text{Cl}:\text{Eu}$ higher matching ability with the flexible PDMS in terms of the interfacial triboelectrification and the electron excitation possibility, and hence the $\text{CaBa}_4(\text{PO}_4)_3\text{Cl}:\text{Eu}/\text{PDMS}$ elastomer can exhibit the highly repeatable and cyclically stable ML during the rapidly and continuously stretching stimuli.

3. Conclusion

In summary, a series of ML elastomers have been constructed by incorporating the CBPOCE solid solutions into the flexible PDMS matrix. Because of the interfacial interactions between the phosphor particles and the polymer chains, the CBPOCE/PDMS elastomers exhibit adjustable ML properties in terms of intensity, spectral characteristics, and repeatability. The $\text{CaBa}_4(\text{PO}_4)_3\text{Cl}:\text{Eu}/\text{PDMS}$ elastomer is confirmed to be the optimum sample, which shows cyan emission with the highest ML intensity. Particularly, the $\text{CaBa}_4(\text{PO}_4)_3\text{Cl}:\text{Eu}/\text{PDMS}$ elastomer exhibits prominent repeatability and cyclic stability that the ML can be maintained for over 20 000 cycles under the rapid and continuous stretching conditions. Based on the investigations in terms of the thermal treatment, matrix effects, triboelectricity, and cathodoluminescence analyses, it is concluded that the ML of the CBPOCE/PDMS composite elastomer should come from both the trap-controlled model and the ITEB model, in which the latter is the real reason for the highly self-activated, stable and repeatable ML. The DFT calculations further reveal that the adjustment of the energy position of VB near the Fermi level and the charge density distribution of the lowest unoccupied band is also responsible for the enhanced ML via solid-solution regulation in addition to the interfacial triboelectricity. This work achieves the intriguing and long-term searching ML elastomer with high

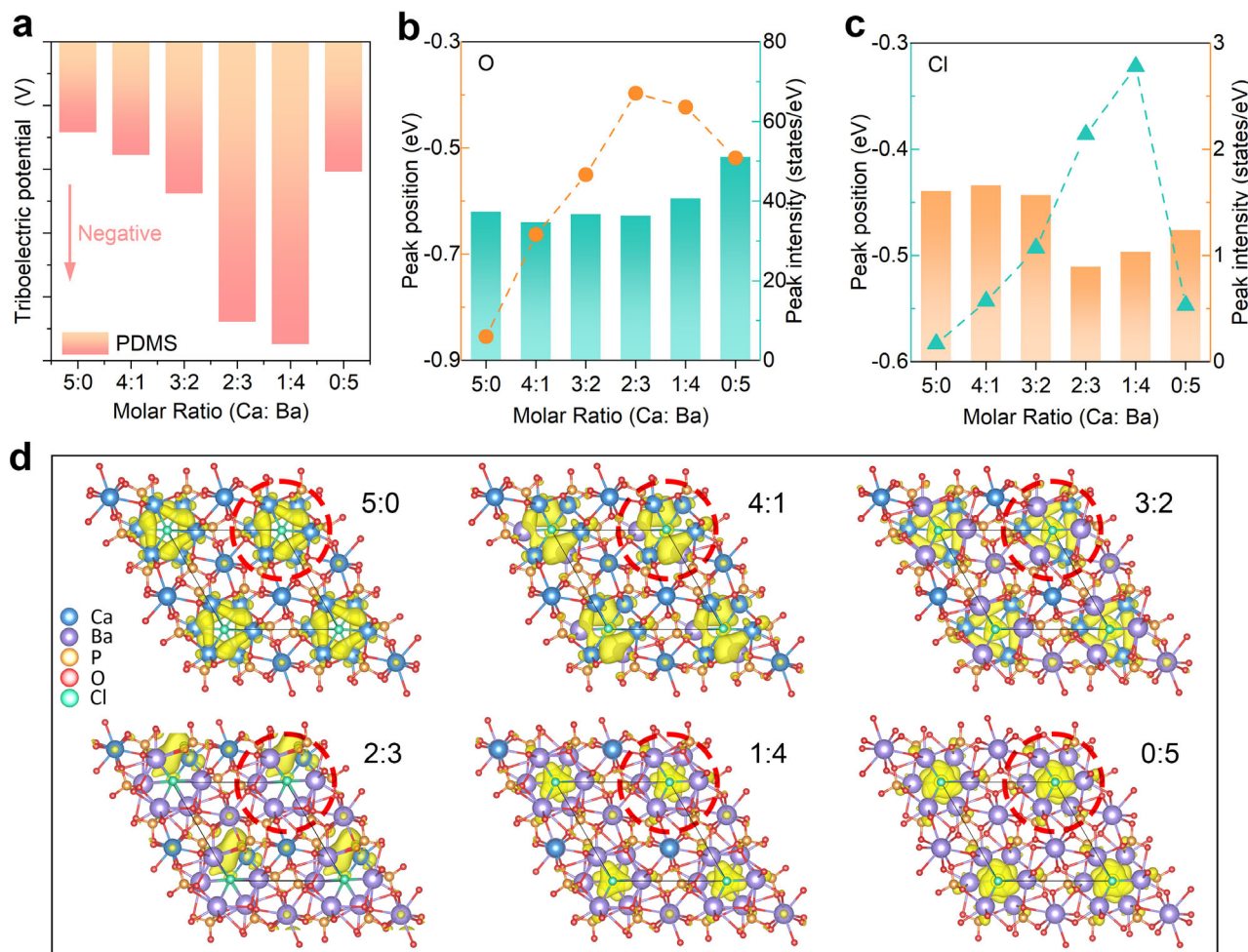


Figure 4. Regulation mechanisms investigation. a) Triboelectric potentials of the PDMS rubbed with the CBPOCE solid solutions. b) Variations of the energy position and peak intensity near the Fermi level from PDOS projected on the O atoms. c) Variations of the energy position and peak intensity near the Fermi level from PDOS projected on the Cl atoms. d) Band-decomposed charge density distributions of the lowest unoccupied band of CBPOCE with various Ca:Ba ratios (isovalue: 0.002 e/Bohr³).

repeatability and cyclic stability after ZnS:Cu/PDMS with disclosed physical principles, which could significantly guide future ML research and promote practical applications in various fields.

4. Experimental Section

Synthesis of CBPOCE Powders: The CBPOCE solid solutions with 0.05 doping content of Eu were synthesized by a solid-state reaction. The CaCO₃ (Aladdin, 99%), BaCO₃ (Aladdin, 99.95%), CaCl₂ (Aladdin, 99.9%), BaCl₂ (Aladdin, 99%), NH₄H₂PO₄ (Aladdin, 99%), and Eu₂O₃ (Aladdin, 99.9%) were employed as raw materials without further purification and weighed with stoichiometric ratios. The raw materials were then mixed in an agate mortar for 0.5 h with the assistance of alcohol. Subsequently, the mixture was transferred into an alumina crucible, and sintered at 1250 °C for 5 h under a reduced atmosphere of 10% H₂ and 90% N₂. After cooling to room temperature, the compounds were ground into powders for further investigation.

Fabrication of the CBPOCE/PDMS Composite Elastomers: The CBPOCE powders were mixed with the PDMS precursor and the curing agent with a weight ratio of 5: 10: 1 in a petri dish with a diameter of 60 mm. The mixture was then placed for 20 min to remove the air. After

that, the mixture was cured in an oven at 70 °C for 30 min, and the CBPOCE/PDMS composite elastomer was obtained. For ML testing and analysis, the as-prepared elastomers were cut into strips with a size of ≈40 × 10 × 1 mm.

Characterizations: The XRD patterns of all samples were measured on a Bruker D2 powder X-Ray diffractometer with Cu K α radiation ($\lambda = 1.5405 \text{ \AA}$, 30 kV, 10 mA). The morphology information and EDS mappings were obtained by an SEM (TESCAN Clara GHM). The PL spectra were acquired using an Omni- λ 300i fluorescence spectrometer with a 500 W Xe 900 lamp as the excitation source. The trap information of the prepared samples was analyzed by the TL measuring equipment (FJ427A1, Beijing Nuclear Instrument Factory). The CL spectrum was obtained through a modified Mp-Micro-S device coupled to SEM. The composite elastomers were stretched on a homemade uniaxial tensile apparatus, and the ML signals were in situ collected and recorded by a fluorescence spectrophotometer (Omni- λ 300i, Zolix Instruments Co., Ltd.) linked to a charge-coupled device (CCD) camera (iVac-316, Edmund Optics Ltd.). The triboelectric potential was measured using a friction tester (MS-T3001, Lanzhou Huahui Instrument Technology Co., Ltd.) equipped with an electrostatic measurement probe (SK050, KEYENCE (Japan) Co., Ltd.).

Density Functional Theory Calculations: All calculations were performed by using the Vienna ab initio simulation package (VASP)^[63,64] based on DFT.^[65,66] The projector augmented wave (PAW)

pseudopotentials were employed to describe interactions between ion cores and valence electrons.^[67] The exchange-correlation energy was treated with the generalized gradient approximation (GGA)^[68] and Perdew–Burke–Ernzerhof (PBE) function. The Brillouin zone was sampled using *k*-points with a spacing of $\approx 0.02 \text{ \AA}^{-1}$ in the Monkhorst–Pack scheme for all theoretical calculations.^[69] The cutoff energy for the plane-wave basis was set at 450 eV. The convergence thresholds for energy and atomic force components were set at 10^{-4} eV and 0.05 eV \AA^{-1} , respectively.

Statistical Analysis: All data was processed by Origin software (Version 2021). To avoid the interference by the interfacial broken and intrinsic traps at the initial stage and show the exact repeatability and stability of the ITEB-induced ML, a pre-stretching of 1000 cycles was applied during the tests in Figure 2b,d,e and Figures S5 and S8 (Supporting Information). For the data in Figures 1f and 3c, no pre-stretching was applied, because it aimed to show the entire cyclic process. The pre-stretching was operated by fixing the CBOPCE/PDMS elastomer on a homemade uniaxial tensile apparatus for 1000 cycles under the frequency of 3 Hz and the strain of 50%. After a certain interval following the pre-stretching, the ML intensity began to be collected continuously. The integration time for ML signal acquisition was set as 100 ms.

Supporting Information

Supporting Information is available from the Wiley Online Library or from the author.

Acknowledgements

This work is supported by the Strategic Priority Research Program of the Chinese Academy of Sciences (XDB 0470201), the Taishan Scholars Program, the Shandong Provincial Natural Science Foundation (ZR2023QB249 and ZR2024QE506), the West Light Foundation of the Chinese Academy of Sciences (xbzg-zdsys-202407), the Key Program of the Natural Science Foundation of Gansu Province (25JRR4471), and the Supporting Fund of Yantai for Leading Researcher.

Conflict of Interest

The authors declare no conflict of interest.

Data Availability Statement

The data that support the findings of this study are available from the corresponding author upon reasonable request.

Keywords

composite elastomer, force-light conversion, mechanoluminescence, repeatability and stability

Received: March 15, 2025

Revised: April 30, 2025

Published online:

[1] Y. Zhuang, R.-J. Xie, *Adv. Mater.* **2021**, *33*, 2005925.

[2] M. C. Wong, L. Chen, G. Bai, L. B. Huang, J. Hao, *Adv. Mater.* **2017**, *29*, 1701945.

- [3] S. M. Jeong, S. Song, K.-I. Joo, J. Kim, S.-H. Hwang, J. Jeong, H. Kim, *Energy Environ. Sci.* **2014**, *7*, 3338.
- [4] N. Terasaki, H. Yamada, C.-N. Xu, *Catal. Today* **2013**, *201*, 203.
- [5] Y. Tang, Y. Cai, K. Dou, J. Chang, W. Li, S. Wang, M. Sun, B. Huang, X. Liu, J. Qiu, L. Zhou, M. Wu, J.-C. Zhang, *Nat. Commun.* **2024**, *15*, 3209.
- [6] Y. Wang, B. Ren, W. Zheng, D. Peng, F. Wang, *Adv. Mater.* **2024**, *36*, 2406899.
- [7] R. R. Petit, S. E. Michels, A. Feng, P. F. Smet, *Light: Sci. Appl.* **2019**, *8*, 124.
- [8] Y. Zhuang, X. Li, F. Lin, C. Chen, Z. Wu, H. Luo, L. Jin, R.-J. Xie, *Adv. Mater.* **2022**, *34*, 2202864.
- [9] L. Guo, P. Xia, T. Wang, A. N. Yakovlev, T. Hu, F. Zhao, Q. Wang, X. Yu, *Adv. Funct. Mater.* **2023**, *33*, 2306875.
- [10] B. Hou, L. Yi, C. Li, H. Zhao, R. Zhang, B. Zhou, X. Liu, *Nat. Electron.* **2022**, *5*, 682.
- [11] S. Hajra, S. Panda, S. Song, B. K. Panigrahi, P. Pakawant, S. M. Jeong, H. J. Kim, *Nano Energy* **2023**, *114*, 108668.
- [12] S. Timilsina, C. W. Jo, K. H. Lee, K.-S. Sohn, J. S. Kim, *Adv. Sci.* **2025**, *12*, 2409384.
- [13] X. Wang, H. Zhang, R. Yu, L. Dong, D. Peng, A. Zhang, Y. Zhang, H. Liu, C. Pan, Z. L. Wang, *Adv. Mater.* **2015**, *27*, 2324.
- [14] H. Li, Y. Yang, P. Li, D. Peng, L. Li, *Adv. Mater.* **2024**, *36*, 2411804.
- [15] X. Fu, Y. Cao, X. Song, R. Sun, H. Jiang, P. Du, D. Peng, L. Luo, *Adv. Funct. Mater.* **2025**, *35*, 2412507.
- [16] H. G. Shin, S. Timilsina, K.-S. Sohn, J. S. Kim, *Adv. Sci.* **2022**, *9*, 2105889.
- [17] H. J. Kim, S. Ji, J. Y. Han, H. B. Cho, Y.-G. Park, D. Choi, H. Cho, J.-U. Park, W. B. Im, *NPG Asia Mater* **2022**, *14*, 26.
- [18] S. Yu, T. H. Park, W. Jiang, S. W. Lee, E. H. Kim, S. Lee, J. E. Park, C. Park, *Adv. Mater.* **2022**, *14*, 2204964.
- [19] L. Su, S. Kuang, Y. Zhao, J. Li, G. Zhao, Z. L. Wang, Y. Zi, *Sci. Adv.* **2024**, *10*, adq8989.
- [20] X. Zhang, Z. Li, W. Du, Y. Zhao, W. Wang, L. Pang, L. Chen, A. Yu, J. Zhai, *Nano Energy* **2022**, *96*, 107115.
- [21] L. Li, C. Cai, X. Lv, X. Shi, D. Peng, J. Qiu, Y. Yang, *Adv. Funct. Mater.* **2023**, *33*, 2301372.
- [22] F. Yang, X. Wu, H. Cui, S. Jiang, Z. Ou, S. Cai, G. Hong, *J. Am. Chem. Soc.* **2022**, *144*, 18406.
- [23] Y. Deng, D. Peng, C.-L. Shen, J. Sun, G. Zheng, S. Chang, Y. Liang, J. He, C.-X. Shan, L. Dong, *Laser Photonics Rev.* **2024**, *18*, 2400251.
- [24] S. Wu, G. Zhou, Y. Wu, P. Xiong, B. Xiao, Z. Zhou, Y. Xiao, P. Shao, S. Wang, Z. Shao, Y. Wang, F. Wang, *Adv. Mater.* **2024**, *36*, 2408508.
- [25] K. Chang, J. Gu, L. Yuan, J. Guo, X. Wu, Y. Fan, Q. Liao, G. Ye, Q. Li, Z. Li, *Adv. Mater.* **2024**, *36*, 2407875.
- [26] J. Guo, F. Guo, H. Zhao, H. Yang, X. Du, F. Fan, W. Liu, Y. Zhang, D. Tu, J. Hao, *Adv. Mater.* **2025**, *37*, 2419405.
- [27] C. Dou, T. Liang, M. Zhao, Z. Song, L. Ning, D. Peng, Q. Liu, *Adv. Funct. Mater.* **2024**, *35*, 2419716.
- [28] J.-C. Zhang, X. Wang, G. Marriott, C.-N. Xu, *Prog. Mater. Sci.* **2019**, *103*, 678.
- [29] H. Zhang, H. Yamada, N. Terasaki, C.-N. Xu, *Appl. Phys. Lett.* **2007**, *91*, 081905.
- [30] X. Yang, R. Liu, X. Xu, Z. Liu, M. Sun, W. Yan, D. Peng, C. N. Xu, B. Huang, D. Tu, *Small* **2021**, *17*, 2103441.
- [31] R. Du, X. He, Y. Xiang, J. Tang, L. Zhou, J. Zhang, T. Sun, M. Wu, *Chem. Eng. J.* **2024**, *499*, 156273.
- [32] W. Li, Y. Cai, J. Chang, S. Wang, J. Liu, L. Zhou, M. Wu, J. C. Zhang, *Adv. Funct. Mater.* **2023**, *33*, 2305482.
- [33] H. I. Jeong, H. S. Jung, C. B. Lee, S. J. Kim, J.-S. Jo, S. Song, S.-J. Ko, D.-W. Kang, S. M. Jeong, J.-W. Jang, K. Kim, J. Lee, H. Choi, *Mater. Today* **2024**, *81*, 4.
- [34] Z. Zheng, Y. Bai, Y. Ren, H. Chen, L. Wu, Y. Kong, Y. Zhang, J. Xu, *J. Mater. Chem. C* **2021**, *9*, 3513.

- [35] S. Liu, Y. Zheng, D. Peng, J. Zhao, Z. Song, Q. Liu, *Adv. Funct. Mater.* **2022**, *33*, 2209275.
- [36] A. Feng, S. Michels, A. Lamberti, W. Van Paepegem, P. F. Smet, *Acta Mater.* **2020**, *183*, 493.
- [37] V. K. Chandra, B. P. Chandra, P. Jha, *Appl. Phys. Lett.* **2013**, *103*, 161113.
- [38] S. M. Jeong, S. Song, S.-K. Lee, B. Choi, *Appl. Phys. Lett.* **2013**, *102*, 051110.
- [39] M.-S. Kim, S. Timilsina, S.-M. Jang, J.-S. Kim, S.-S. Park, *Adv. Mater. Technol.* **2024**, *9*, 2400255.
- [40] X. Y. Wei, H. L. Wang, Y. Wang, S. Y. Kuang, X. X. Zhu, J. Zou, L. Wang, X. Zeng, F. Rao, G. Zhu, *Nano Energy* **2019**, *61*, 158.
- [41] K.-S. Sohn, S. Timilsina, S. P. Singh, T. Choi, J. S. Kim, *APL Mater.* **2016**, *4*, 106102.
- [42] G. Lee, S. Song, W. H. Jeong, C. Lee, J.-S. Kim, J.-H. Lee, J. Choi, H. Choi, Y. Kim, S. J. Lim, S. M. Jeong, *Small* **2024**, *20*, 2307089.
- [43] H. I. Jeong, H. S. Jung, M. Dubajic, G. Kim, W. H. Jeong, H. Song, Y. Lee, S. Biswas, H. Kim, B. R. Lee, J. W. Yoon, S. D. Stranks, S. M. Jeong, J. Lee, H. Choi, *Nat. Commun.* **2025**, *16*, 854.
- [44] W. Wang, S. Wang, Y. Gu, J. Zhou, J. Zhang, *Nat. Commun.* **2024**, *15*, 2014.
- [45] M. Wang, J. Xiao, J. Zhang, L. Zhao, Y. Song, Z. Liu, T. Wang, X. Xu, J. Yu, *Chem. Eng. J.* **2024**, *502*, 157876.
- [46] X. Pan, Y. Zhuang, W. He, C. Lin, L. Mei, C. Chen, H. Xue, Z. Sun, C. Wang, D. Peng, Y. Zheng, C. Pan, L. Wang, R.-J. Xie, *Nat. Commun.* **2024**, *15*, 2673.
- [47] Y. Bai, F. Wang, L. Zhang, D. Wang, Y. Liang, S. Yang, Z. Wang, *Nano Energy* **2022**, *96*, 107075.
- [48] Y. Bai, X. Guo, B. Tian, Y. Liang, D. Peng, Z. Wang, *Adv. Sci.* **2022**, *9*, 2203249.
- [49] Z. Ma, Y. Han, Y. Bai, B. Liu, Z. Wang, *Chem. Eng. J.* **2023**, *456*, 141122.
- [50] S. Qin, W. Wei, B. Tian, Z. Ma, S. Fang, Y. Wang, J. Zhang, Z. Wang, *Adv. Funct. Mater.* **2024**, *34*, 2401535.
- [51] Z. Ma, S. Fang, Y. Bai, W. Wei, Z. Wang, *Mater. Today Chem.* **2024**, *36*, 101917.
- [52] K. Cheng, Z. Guo, P. Zhang, L. Feng, Y. Zhou, L. Li, H. Song, T. Wang, Y. Zhao, L. Zhao, *Laser Photonics Rev.* **2025**, *19*, 2401524.
- [53] I. M. Nagpure, S. S. Pitale, E. Coetsee, O. M. Ntwaeaborwa, J. J. Terblans, H. C. Swart, *Physica B* **2012**, *407*, 1505.
- [54] H. Kageyama, K. Hayashi, K. Maeda, J. P. Attfield, Z. Hiroi, J. M. Rondinelli, K. R. Poeppelmeier, *Nat. Commun.* **2018**, *9*, 772.
- [55] C. Chen, Y. Zhuang, D. Tu, X. Wang, C. Pan, R.-J. Xie, *Nano Energy* **2020**, *68*, 104329.
- [56] X. Zhang, H. Suo, Y. Guo, J. Chen, Y. Wang, X. Wei, W. Zheng, S. Li, F. Wang, *Nat. Commun.* **2024**, *15*, 6797.
- [57] Y. Chen, Z. Yang, J. Jin, J. Qiao, Y. Wang, M. S. Molokeev, H. C. Swart, Z. Xia, *Chem. Mater.* **2023**, *35*, 8714.
- [58] S. Zhou, Y. Cheng, J. Xu, H. Lin, Y. Wang, *Adv. Funct. Mater.* **2022**, *32*, 2208919.
- [59] Z.-C. Wu, F.-F. Wang, K. Zhang, S.-C. Xu, J. Liu, Z. Xia, M.-M. Wu, *Dyes Pigments* **2018**, *150*, 275.
- [60] S. Liu, R. Liu, X. Yang, J. Li, M. Sun, C.-N. Xu, B. Huang, Y. Liang, D. Tu, *Nano Energy* **2022**, *93*, 106799.
- [61] Y. He, J. Wang, S. Fang, J. Qin, L. Feng, B. Tian, S. Feng, Z. Wang, *J. Mater. Chem. C* **2025**, *13*, 6588.
- [62] Y. Hua, W. Ran, J. S. Yu, *Chem. Eng. J.* **2021**, *406*, 127154.
- [63] G. Kresse, J. Furthmüller, *Phys. Rev. B* **1996**, *54*, 11169.
- [64] G. Kresse, J. Furthmüller, *Comp. Mater. Sci.* **1996**, *6*, 15.
- [65] P. Hohenberg, W. Kohn, *Phys. Rev.* **1964**, *136*, B864.
- [66] X. Gonze, P. Ghosez, R. W. Godby, *Phys. Rev. Lett.* **1997**, *78*, 294.
- [67] P. E. Blöchl, *Phys. Rev. B* **1994**, *50*, 17953.
- [68] J. P. Perdew, K. Burke, M. Ernzerhof, *Phys. Rev. Lett.* **1997**, *78*, 1396.
- [69] D. J. Chadi, *Phys. Rev. B* **1977**, *16*, 1746.